

Electronic Supplementary Information

Soft template-assisted design and synthesis of anisotropic 2D-3D CuInS₂ with controlled morphology and band gap: exploring photothermal interfacial water evaporation

Ashok Barhoi, Bhagirath Mahto, Haider Ali, and Sahid Hussain*

Department of Chemistry Indian Institute of Technology Patna, Bihta, 801106, Bihar, India

*Email: sahid@iitp.ac.in; Phone: +91-6115-233022

General Consideration

Text S1. Materials used

Copper acetate (Cu(CH₃COO)₂, ≥99.00%) and indium acetate (In(CH₃COO)₃, ≥99.99%) were sourced from Sigma Aldrich, while polyethylene glycol-400 (PEG-400) was purchased from Chemical Drug House, (P) Ltd. (New Delhi, India). Thiourea (NH₂CSNH₂, ≥99.0%) was obtained from Tokyo Chemical Industry Co. Ltd. (Tokyo, Japan). All chemicals were used as received, without further purification.

Text S2. Methods

Text S2.1 Material Characterization

The recording of powder X-ray diffraction (P-XRD) data in the 2θ range of 10–80° employed a PANalytical X-ray diffractometer with Cu Kα radiation (λ = 1.5406 Å) at 45 kV and 40 mA. Raman spectroscopy utilized a Lab Ram HR800 UV Raman microscope (Horiba Jobin-Yvon, France), and a UV–vis-NIR spectrophotometer (Shimadzu UV-NIR-3600), is utilized for band gap determination. Microscopic imaging for field emission scanning electron microscopy (FE-SEM) was conducted using a Zeiss Gemini SEM500 instrument equipped with an EDS detector. Additionally, transmission electron microscopy (TEM) and high-resolution TEM (HR-TEM) micrographs were acquired using a JEOL JEM 200 electron microscope operating at 200 kV. X-ray photoelectron spectra (XPS) were acquired using a Thermo Fisher Scientific

ESCALAB XI⁺ X-ray photoelectron spectrometer featuring a Mg K α excitation source. The determination of Brunauer–Emmett–Teller (BET) specific surface area and porosity involved the analysis of N₂ adsorption-desorption isotherm curves using a Quantachrome Autosorb iQ2 analyzer.

Text S2.2 Photothermal study

The solar-driven evaporation performance was assessed using a custom-built solar-thermal device in the lab. A water-filled beaker was topped with circular insulation foam to ensure insulation and block direct sunlight, preventing it from affecting the experimental results. A hydrophilic paper was inserted through the foam's center hole as a water supply channel. The prepared powder sample was first dispersed in 2 mL of water using an ultrasonic method, then the slurry was evenly coated on the top of the sponge with an effective area of 2 cm x 2 cm, and thickness of the evaporator is measured as 1.5(\pm 2) cm, with 7(\pm 2) mm layer of material loading. with sample loading of 40 mg. The experimental environment was maintained at approximately 25 °C. A solar simulator (71S0503A) with a solar flux of 1 kW m⁻² (1 sun) was placed over the evaporator. An infrared thermal imaging camera (FLIR E4) monitored the temperature changes on the sample surface throughout the solar photothermal water evaporation experiments. Water mass changes were recorded using an electronic analytical balance (FA324C) with a precision of 0.001 g.

Text S2.3 Electrochemical study

Mott-Schottky measurements were conducted using a three-electrode setup, using Metrohm Autolab M101 instrument, NOVA 2.1.5 software equipped with an Ag/AgCl electrode as the reference, a platinum wire as the counter electrode, and the active material serving as the working electrode. The working electrodes were prepared on fluorine-doped tin oxide (FTO) substrates by drop-casting a thin film of CuInS₂ paste. The slurry for the paste was made by mixing 10 mg of CuInS₂ with 60 μ L of Nafion, 100 μ L of distilled water, and 140 μ L of ethanol,

followed by 30 minutes of sonication to achieve a homogeneous mixture. A 0.5 M Na₂SO₄ solution was used as the electrolyte.

Note S1. Evaporation rate calculations:

$$m = \frac{(M_1 - M_2)}{tS}$$

Where, evaporation rate, denoted as m, is calculated using M₁, which represents the water mass loss under 1 sun illumination, and M₂, which indicates the self-evaporation of water in the dark. M₂ is determined by subtracting the water mass loss without CIS (13 mg) from the mass loss with CIS in dark conditions (26 mg, 23 mg, and 24 mg for CIS-1, CIS-2, and CIS-3, respectively). Variables t and S represent the illumination time and evaporation area (4 cm²).

Sample name	Formula	M ₁ (initial-final) (gm)	M ₂ (gm)	Time (t) (hour)	Absorber Surface area (10 ⁻⁴ *m ²)	Rate (kg m ⁻² h ⁻¹)
CIS-1	$m = \frac{(M_1 - M_2)}{tS}$	(135.12-134.5)	(0.026-0.013)	1	4	1.55
CIS-2		(135.12-134.56)	(0.023-0.013)			1.38
CIS-3		(135.12-134.53)	(0.024-0.013)			1.45

Note S2. Efficiency calculation

The efficiency (η) has been calculated using the following equation

$$\eta = \frac{mh_{LV}}{I}$$

Here, m signifies the mass flux (evaporation rate) with units of kg m⁻²h⁻¹, h_{LV} denotes the enthalpy change associated with the liquid-vapor phase transition, valued at 2250 kJ kg⁻¹, and I represent the power density of solar radiation, equal to 1 kW m⁻².

Sample name	Formula	m (Rate) (kg m ⁻² h ⁻¹)	h _{LV} (kg m ⁻² h ⁻¹)	Intensity (I) (kWm ⁻²)	Efficiency (%)
CIS-1	$\eta = \frac{mh_{LV}}{I}$	1.55	2250	1	96
CIS-2		1.38			86
CIS-3		1.45			91

Note S3. Water Evaporation Enthalpy Calculation

Based on the dark evaporation experiments presented in **Fig. S11**, the water losses in the presence of CIS-1, CIS-2, and CIS-3 were 26 mg, 23 mg, and 24 mg, respectively, while the control sample (without CIS) showed a water loss of only 13 mg under similar conditions. The theoretical evaporation enthalpy of liquid water is about 2.434 kJ g⁻¹. Hence, the equivalent water evaporation enthalpy for water in CIS can be evaluated using the formula provided below:

$$U_{in} = E_{eqv}m_g = E_0m_0$$

Here, U_{in} refers to the total energy input from the environment per hour, E_0 and m_0 are the water evaporation enthalpy (kJ g⁻¹) and the mass loss (g) of bulk water in darkness over 1 hour, respectively, and m_g indicates the water loss (g) of water in CIS, and E_{eqv} represents the equivalent water evaporation enthalpy (kJ g⁻¹). The corresponding obtained E_{eqv} values are 1.21 kJ g⁻¹, 1.37 kJ g⁻¹, and 1.32 kJ g⁻¹ which are 50.28%, 43.71%, and 45.76% lower than the theoretical evaporation enthalpy of pure water (2.434 kJ g⁻¹).

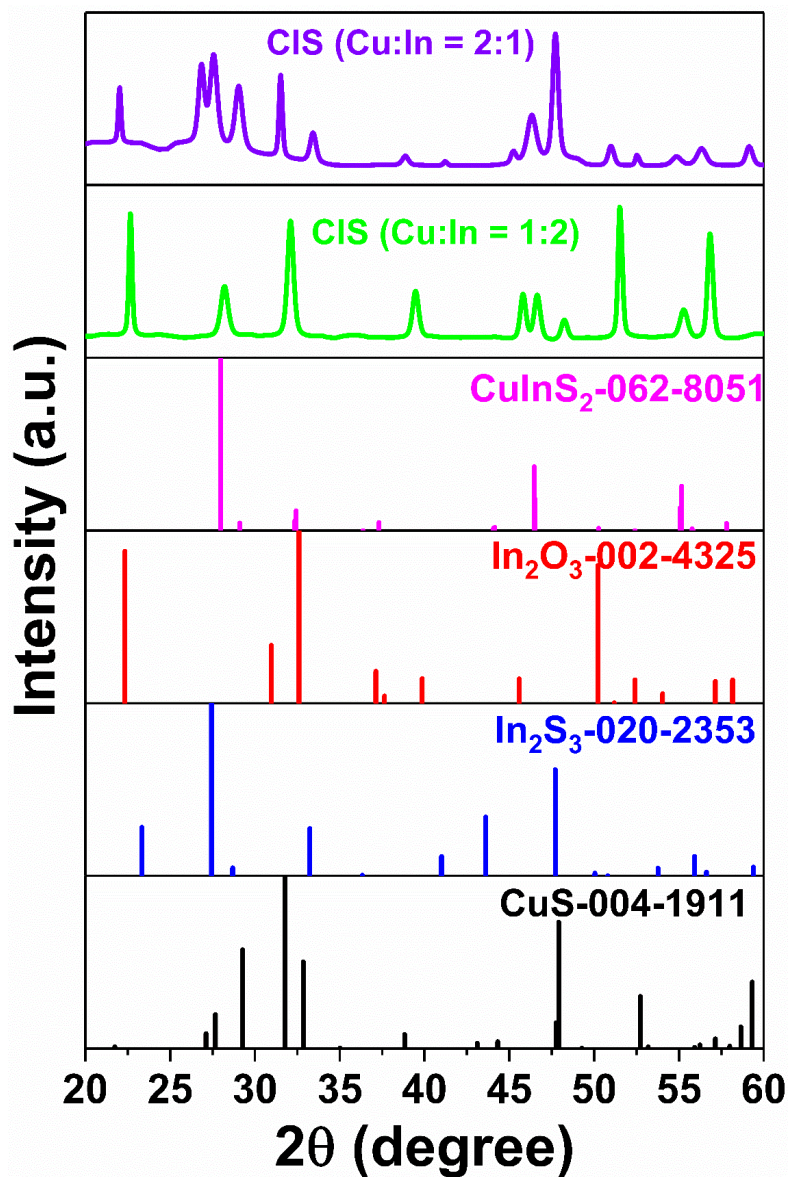


Fig. S1 P-XRD patterns of CuInS_2 synthesized with Cu: In in 1:2 and 2:1.

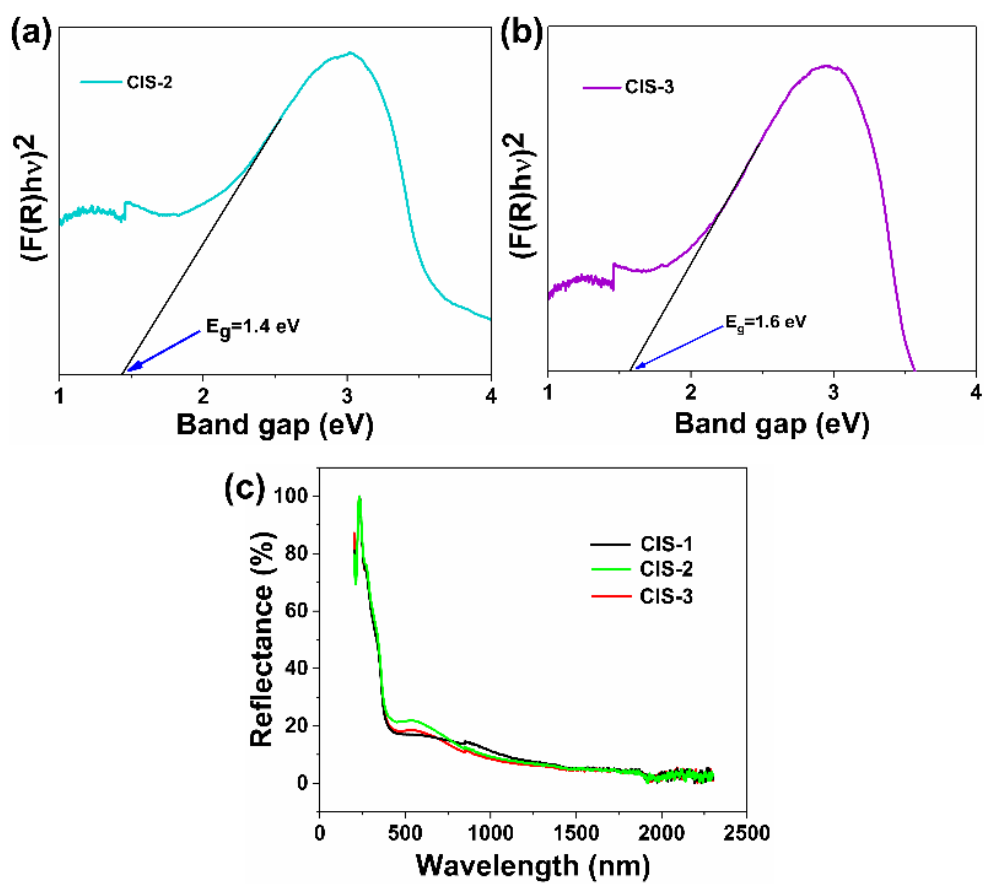


Fig. S2 UV-DRS spectra plots of (a) CIS-2, (b) CIS-3; (c) Full range reflectance spectra of CIS-1, CIS-2 and CIS-3.

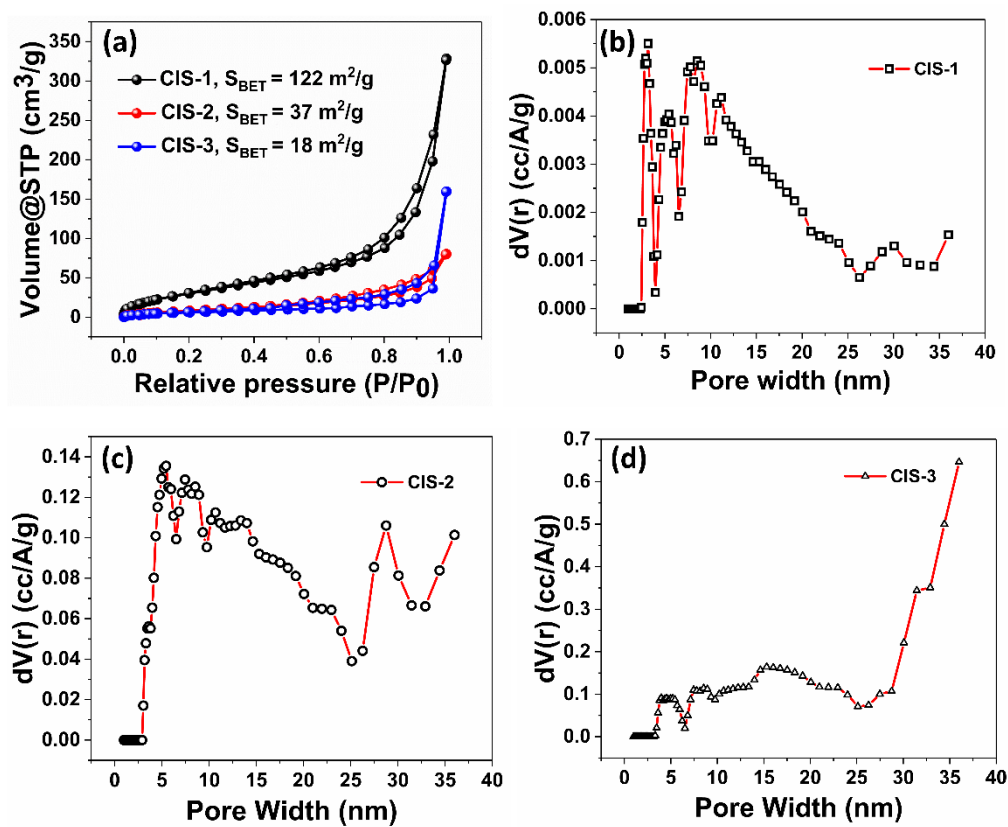


Fig. S3 (a) N_2 adsorption-desorption isotherms; pore-width distribution plots of (b) CIS-1, (c) CIS-2, (d) CIS-3.

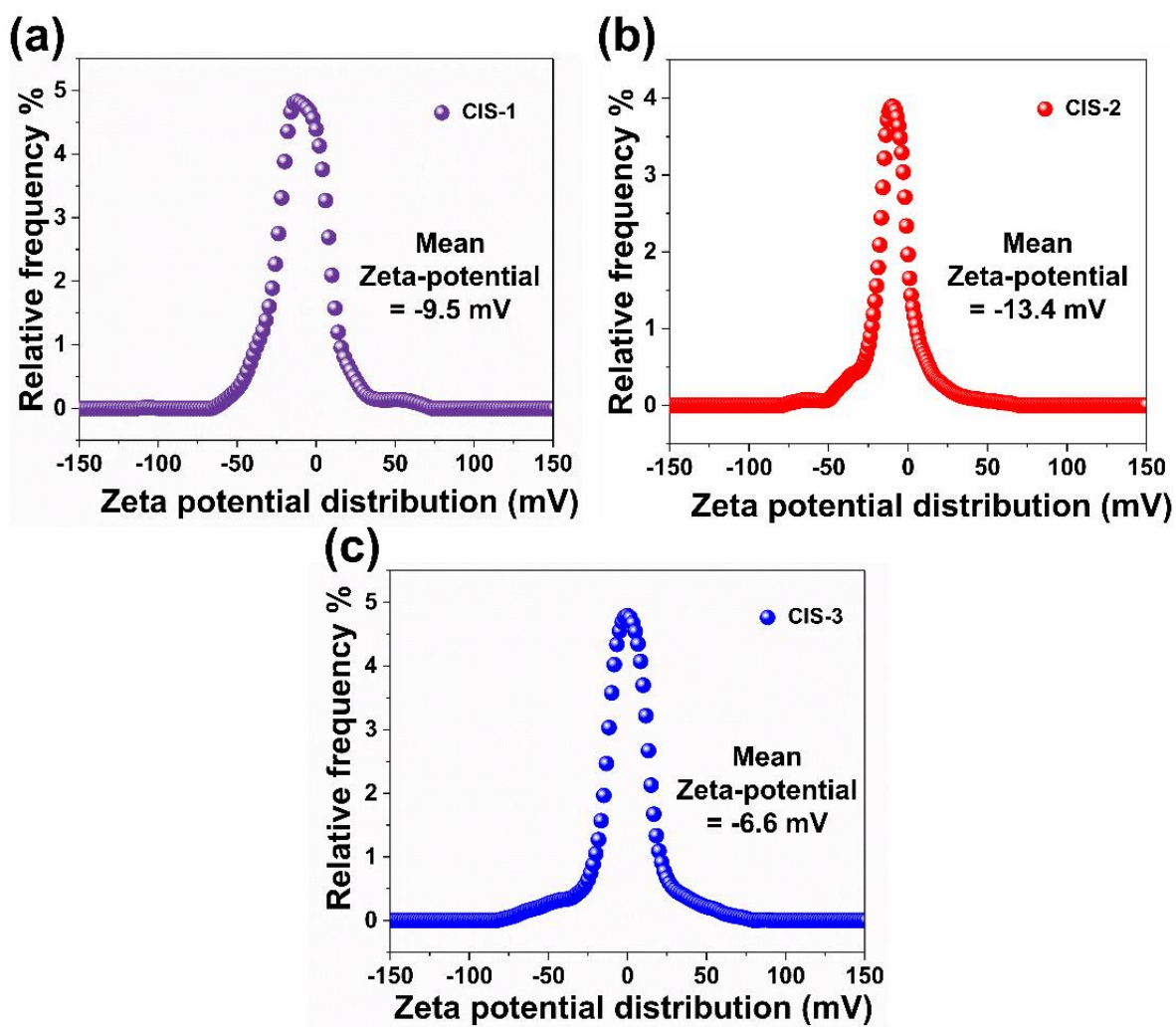


Fig. S4 Zeta-potential of (a) CIS-1, (b) CIS-2, (c) CIS-3.

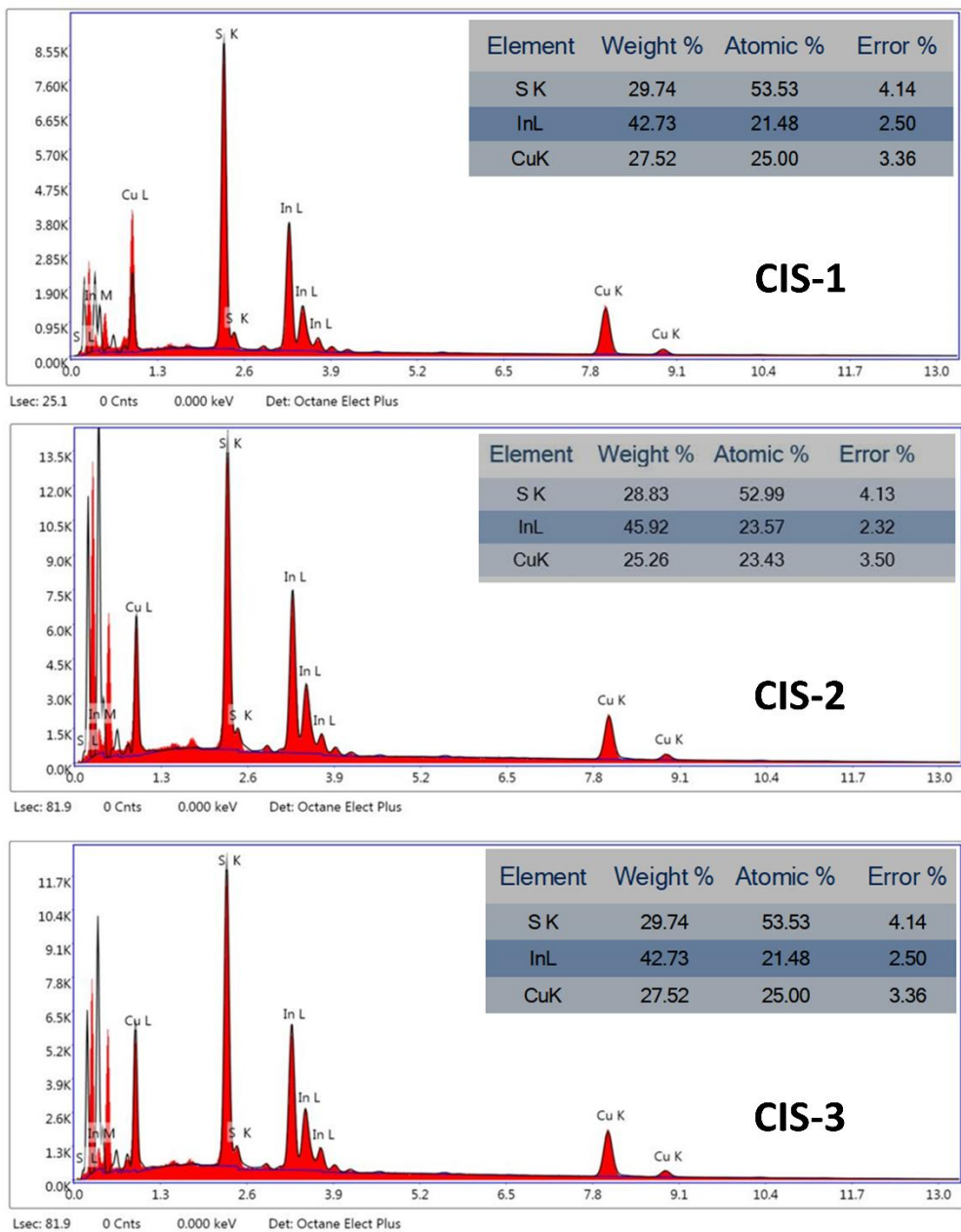


Fig. S5 EDS elemental line mapping spectrum (a) CIS-1, (b) CIS-2, (c) CIS-3.

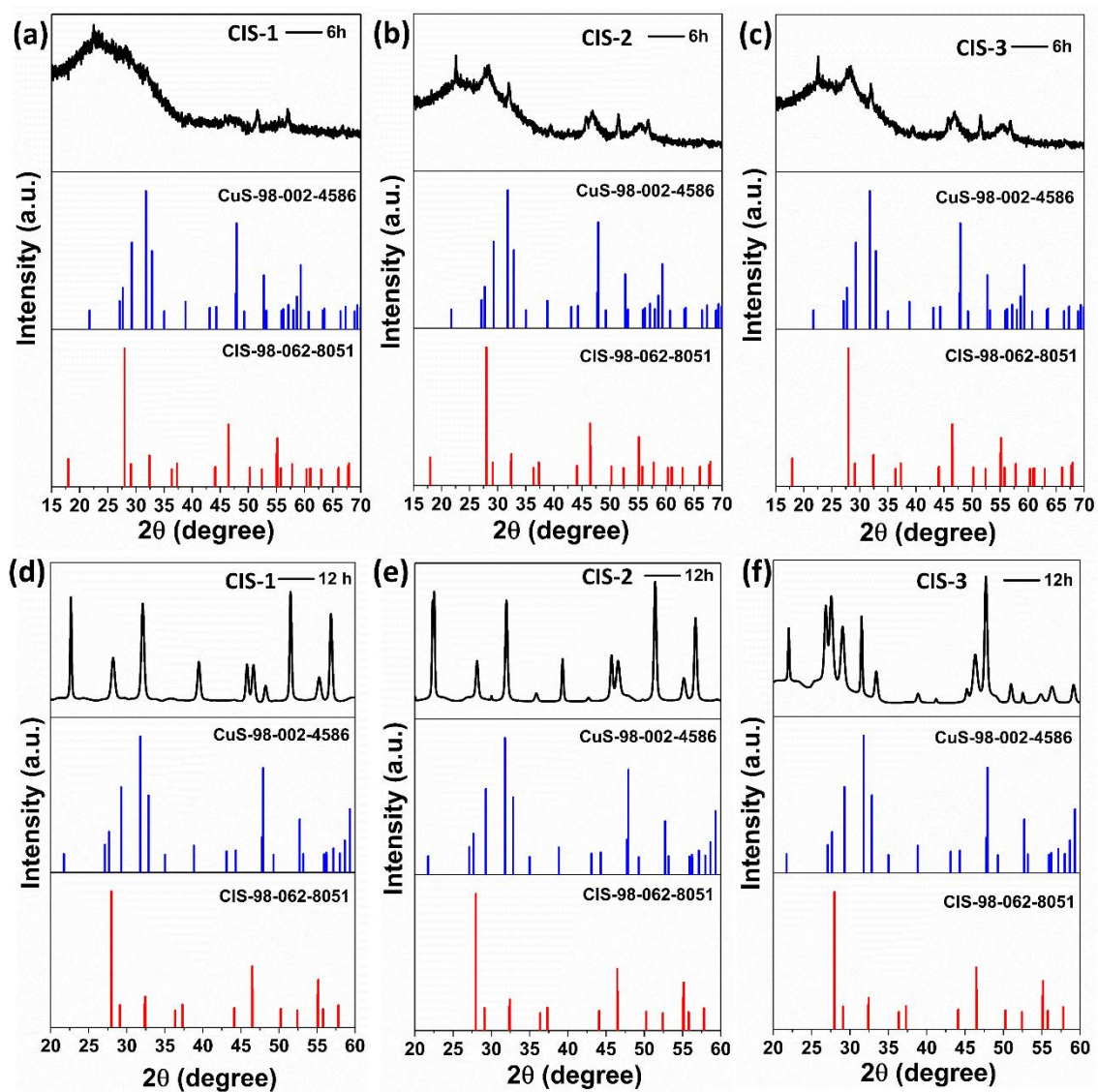


Fig. S6 P-XRD patterns of CIS-1 (a) 6 h, (d) 12 h; CIS-2 (b) 6 h, (e) 12 h; CIS-3 (c) 6 h, (f) 12 h.

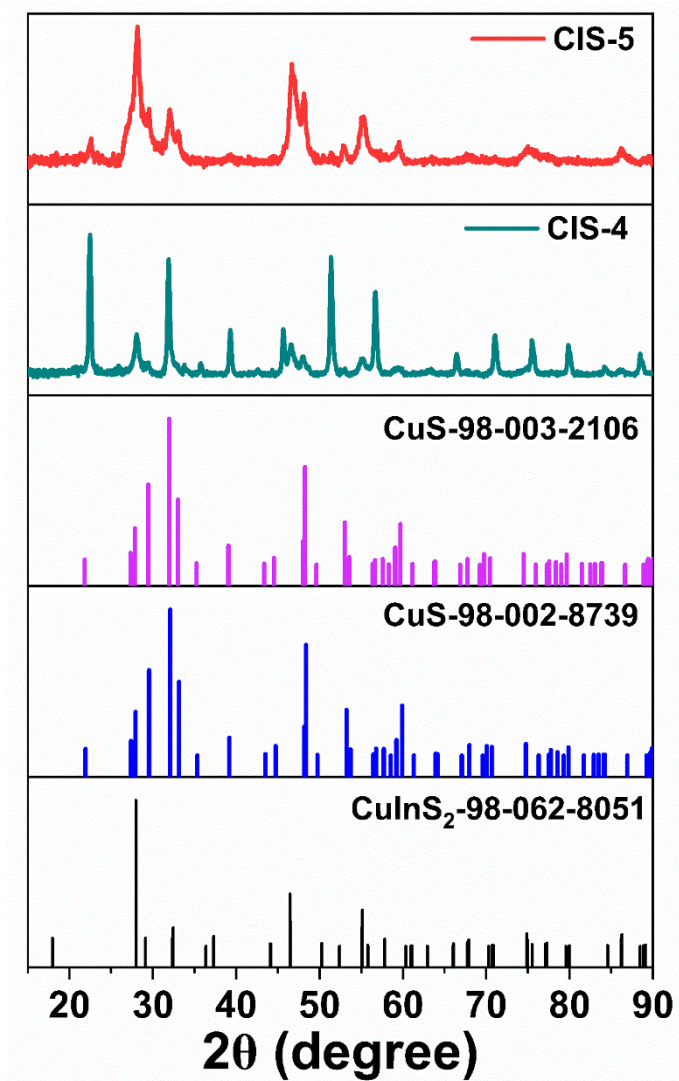


Fig. S7 P-XRD patterns of CIS-4 and CIS-5.

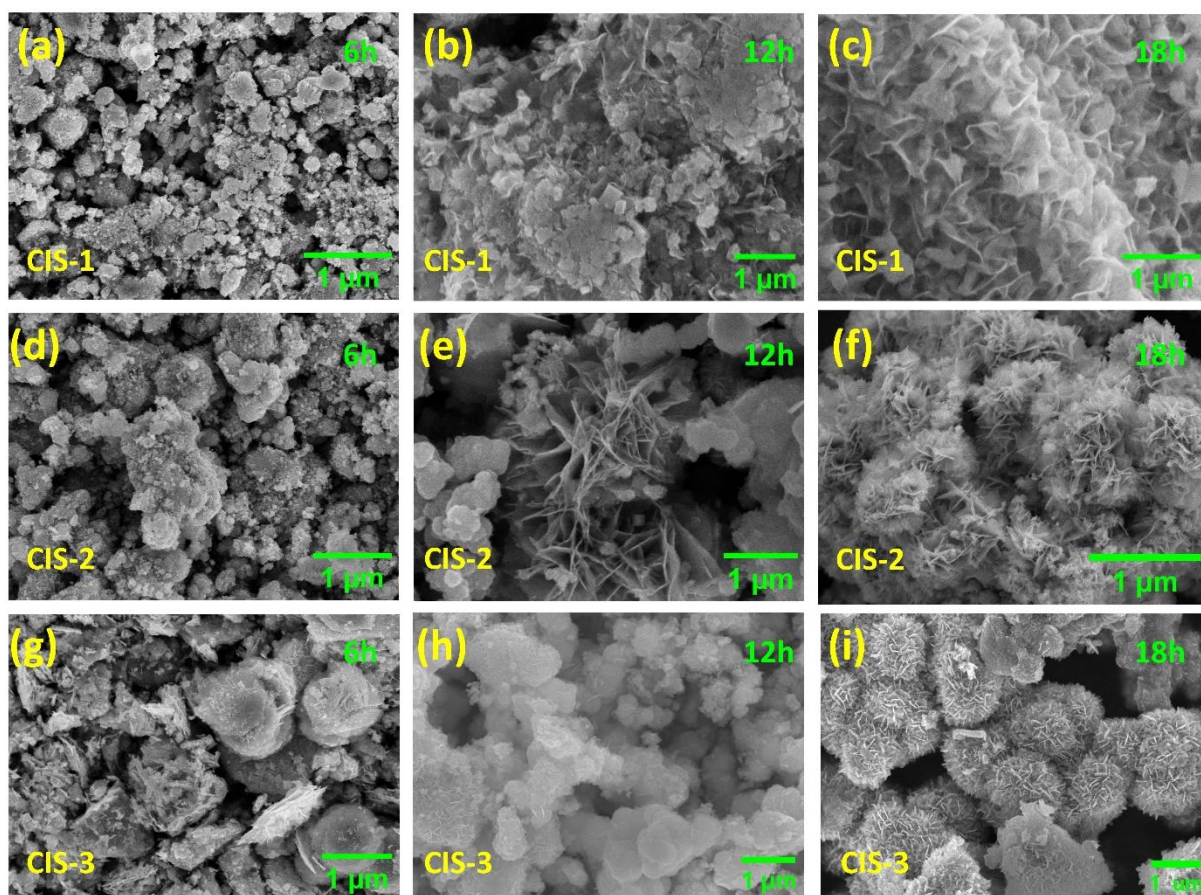


Fig. S8 FE-SEM micrographs of CIS-1 (a) 6 h, (b) 12 h, (c)18 h; CIS-2 (d) 6 h, (e)12 h, (f) 18 h, and CIS-3 (g) 6 h, (h) 12 h, and (i) 18 h.

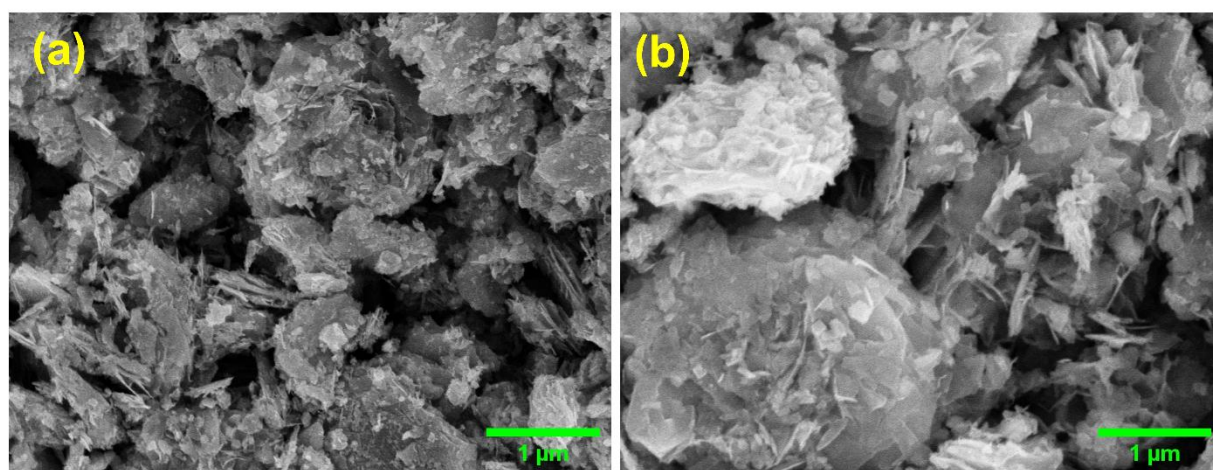
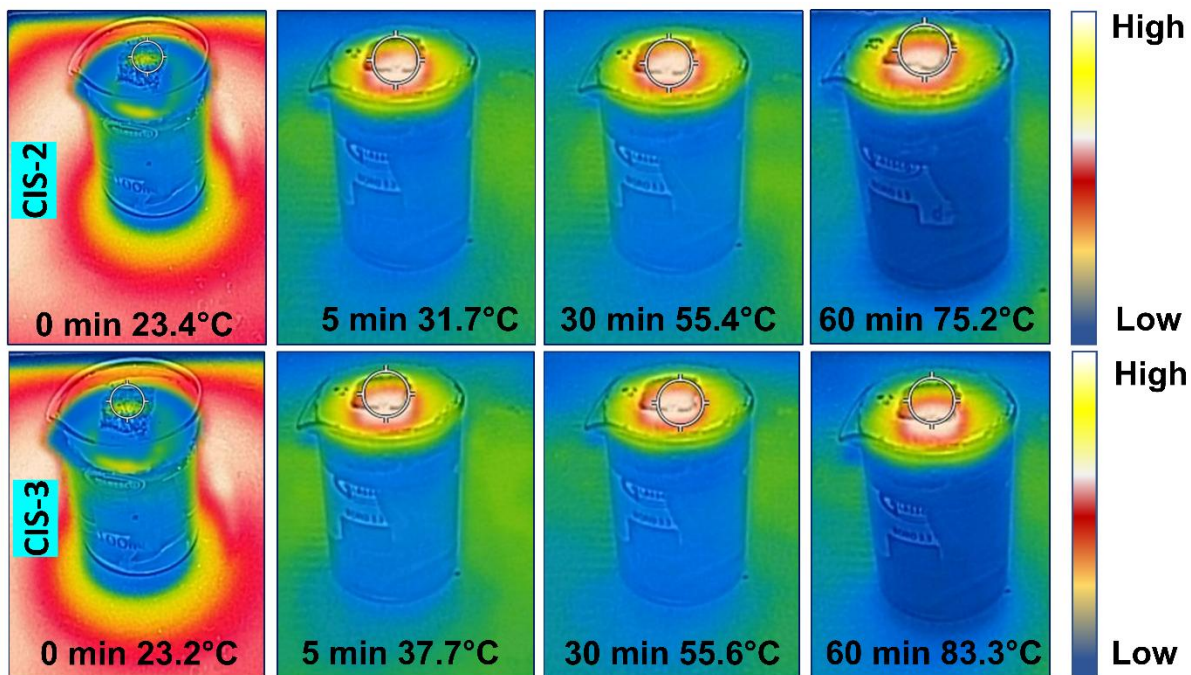


Fig. S9 FE-SEM micrographs of (a) CIS-4, and (b) CIS-5.



ig. S10. Infrared thermal images showing the surface temperatures of the CIS-2 and CIS-3 samples at various irradiation times.

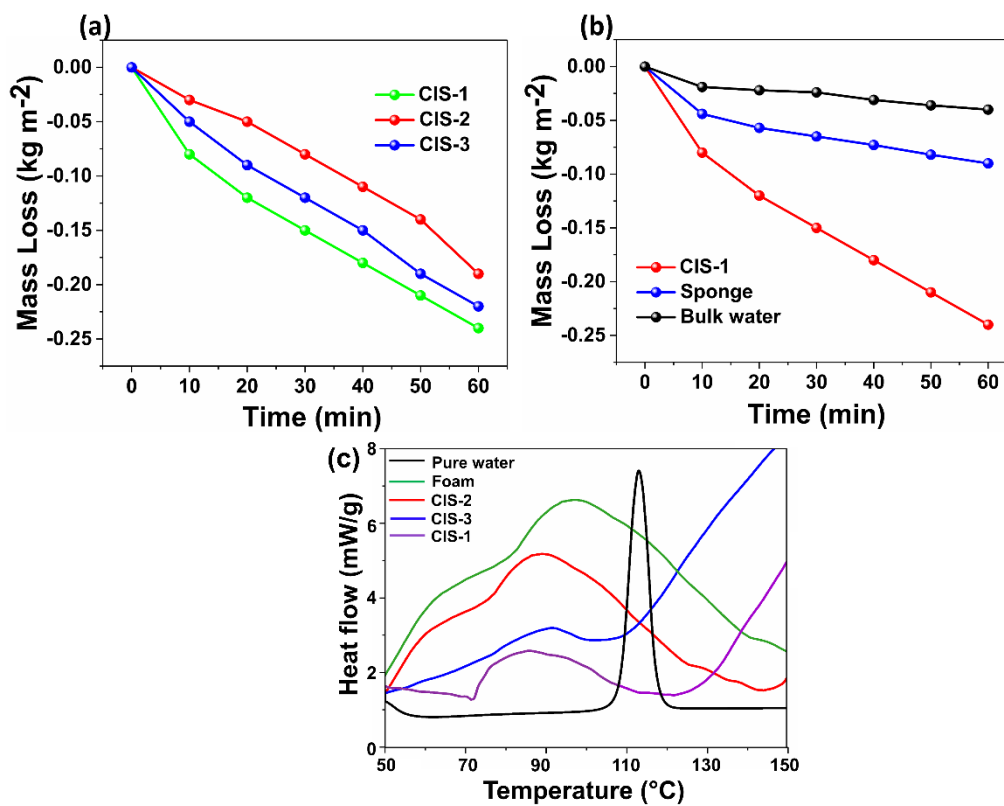


Fig. S11. Dark evaporation experiments of (a) CIS, (b) bulk water, sponge, and CIS-1 systems, (c) DSC curves for CIS-1, CIS-2, and CIS-3.

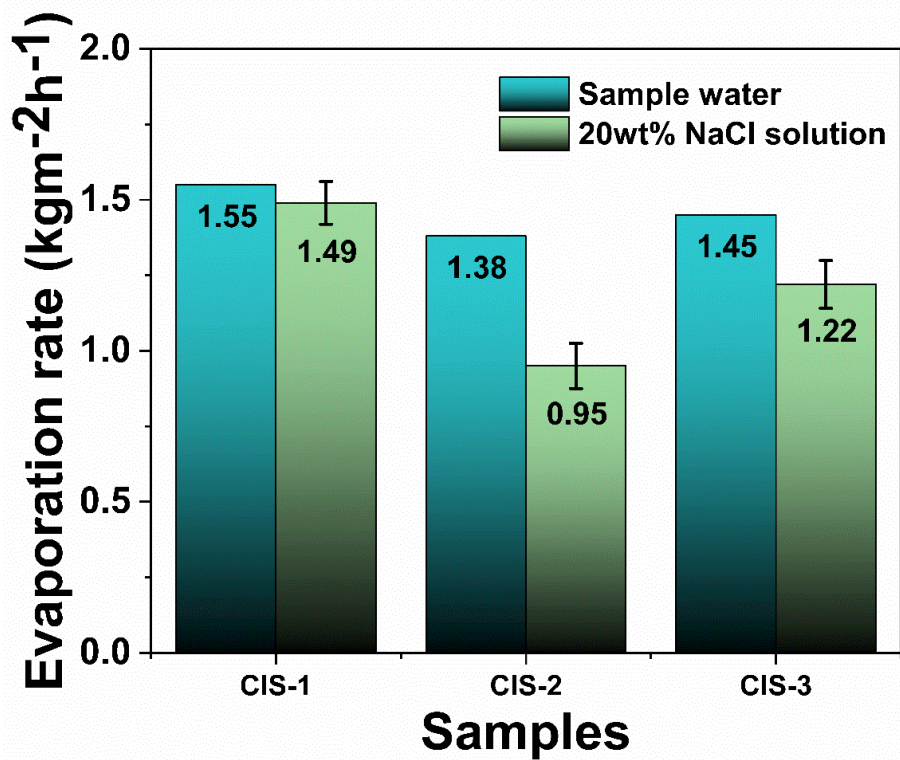


Fig. S12 (a) Bar diagram representing evaporation rate for 20% NaCl water.

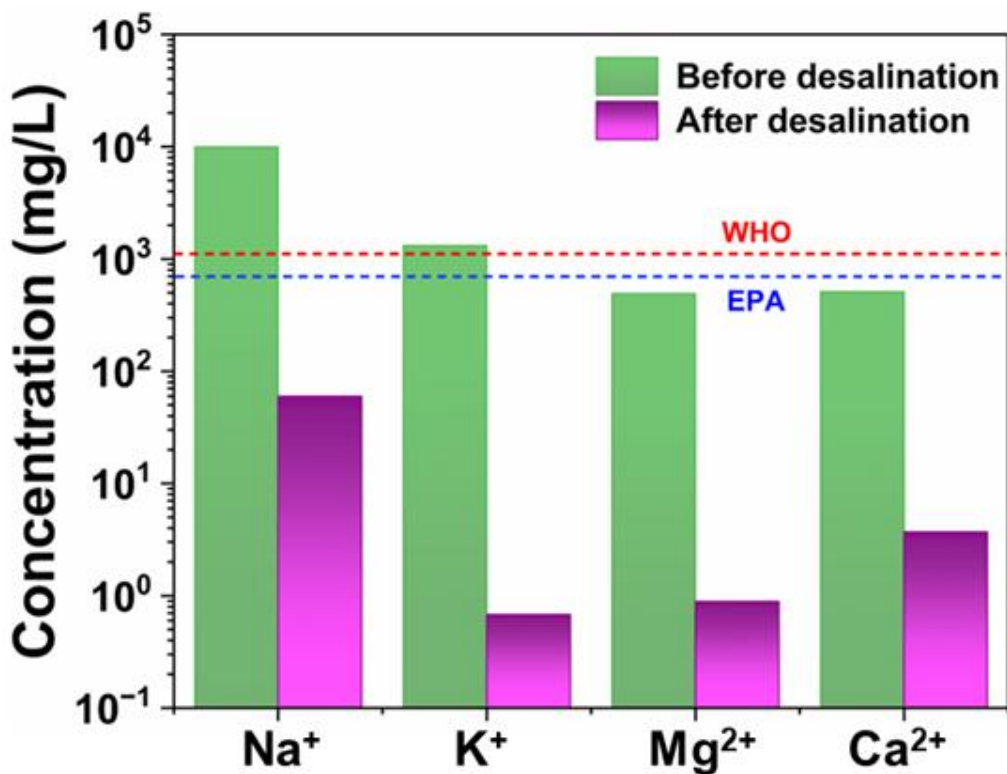


Fig. S13 Ion concentrations of brine before and after desalination.

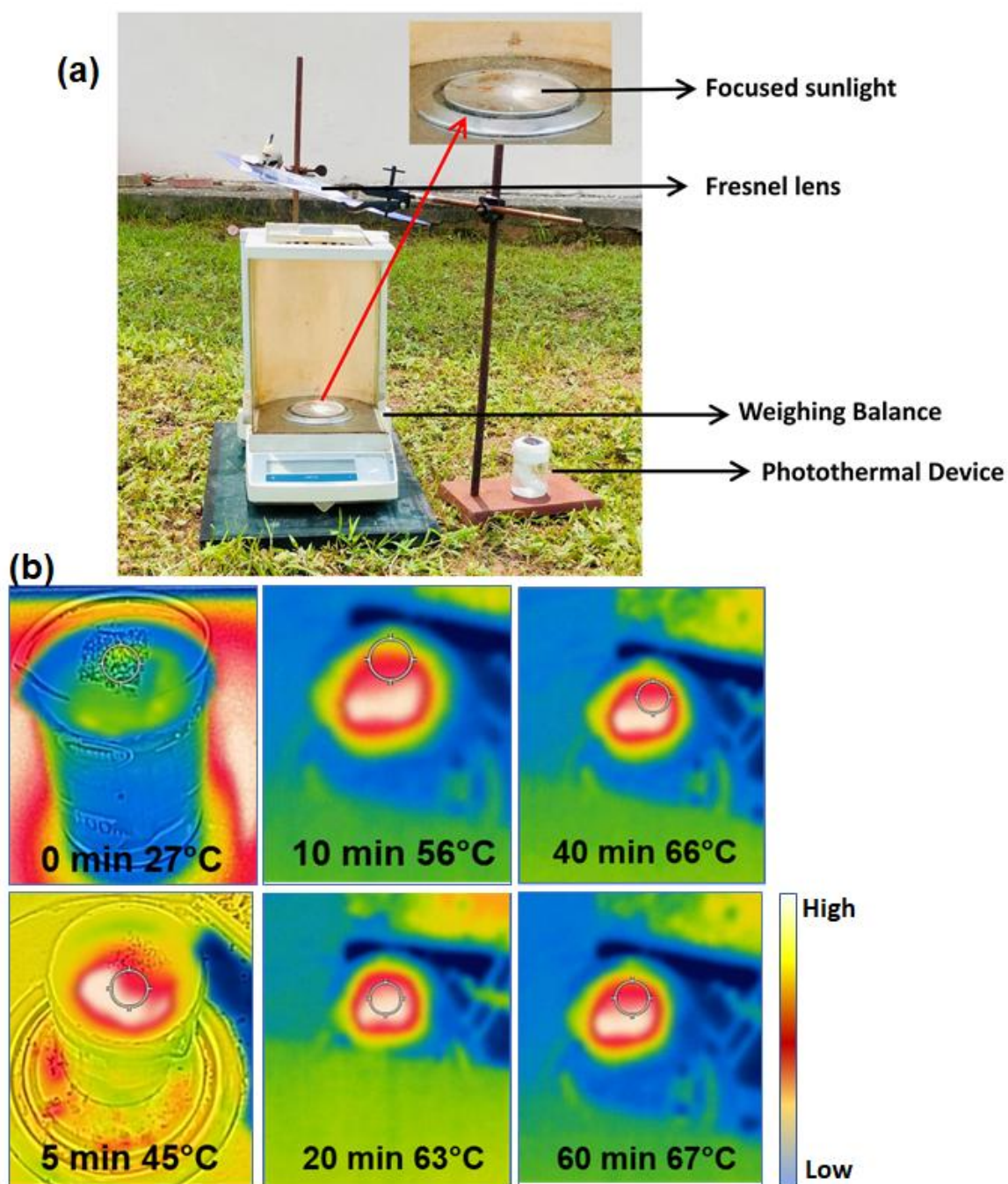


Fig. S14(a) Outdoor photothermal water evaporation experimental setup during the daytime, and (b) Real-time infrared thermal images of the outdoor experiment.

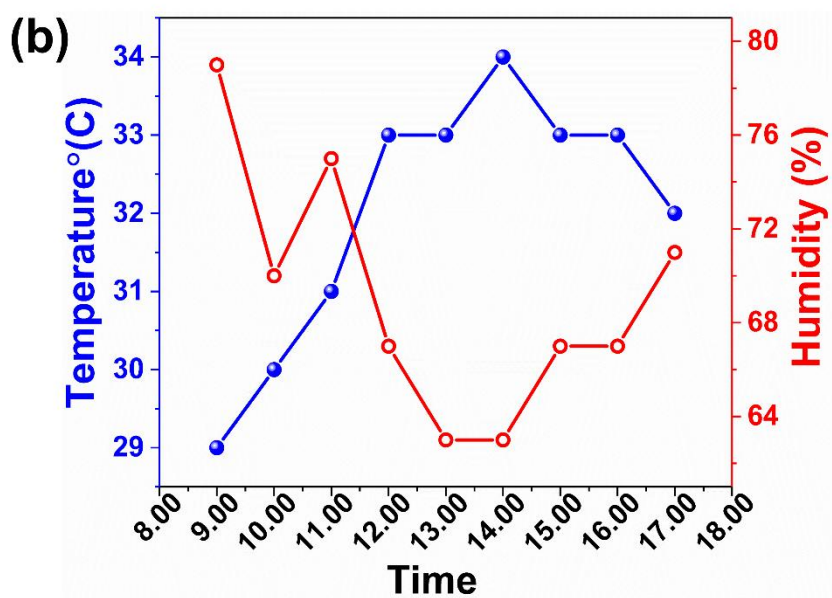
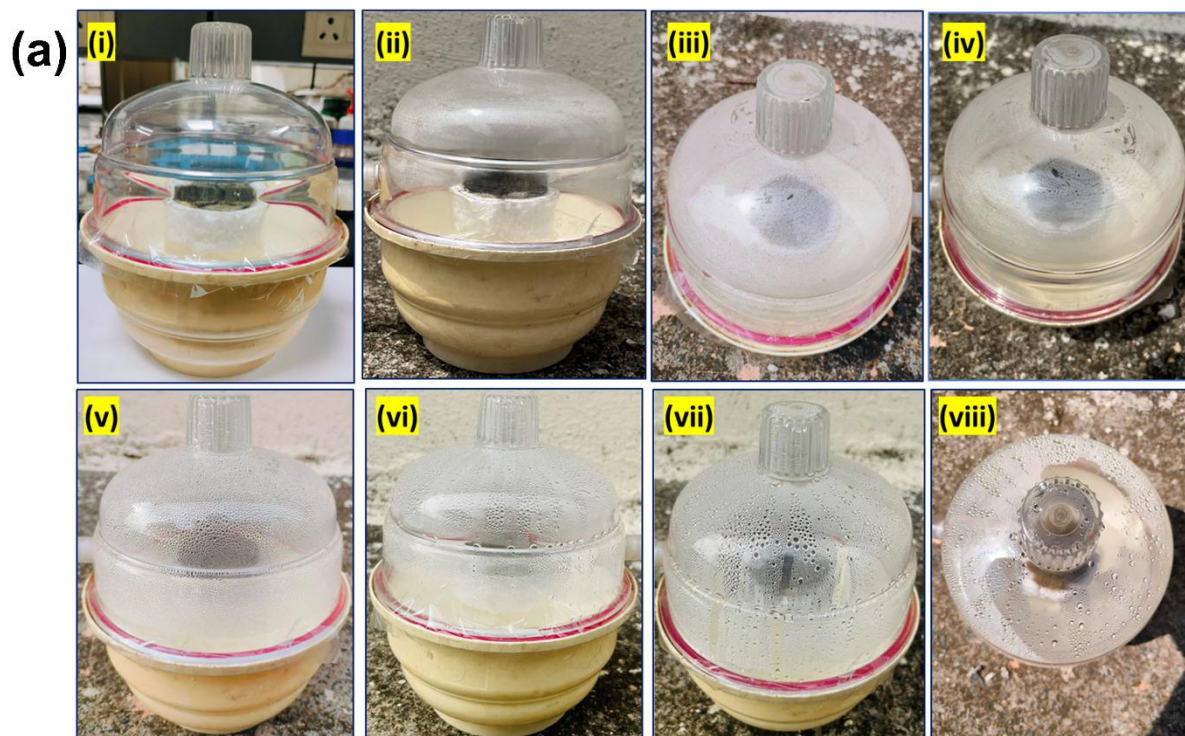


Fig. S15 (a) Digital images of the large-scale photothermal setup evaporation/condensation with time, (b) temperature and humidity vs. time plot.

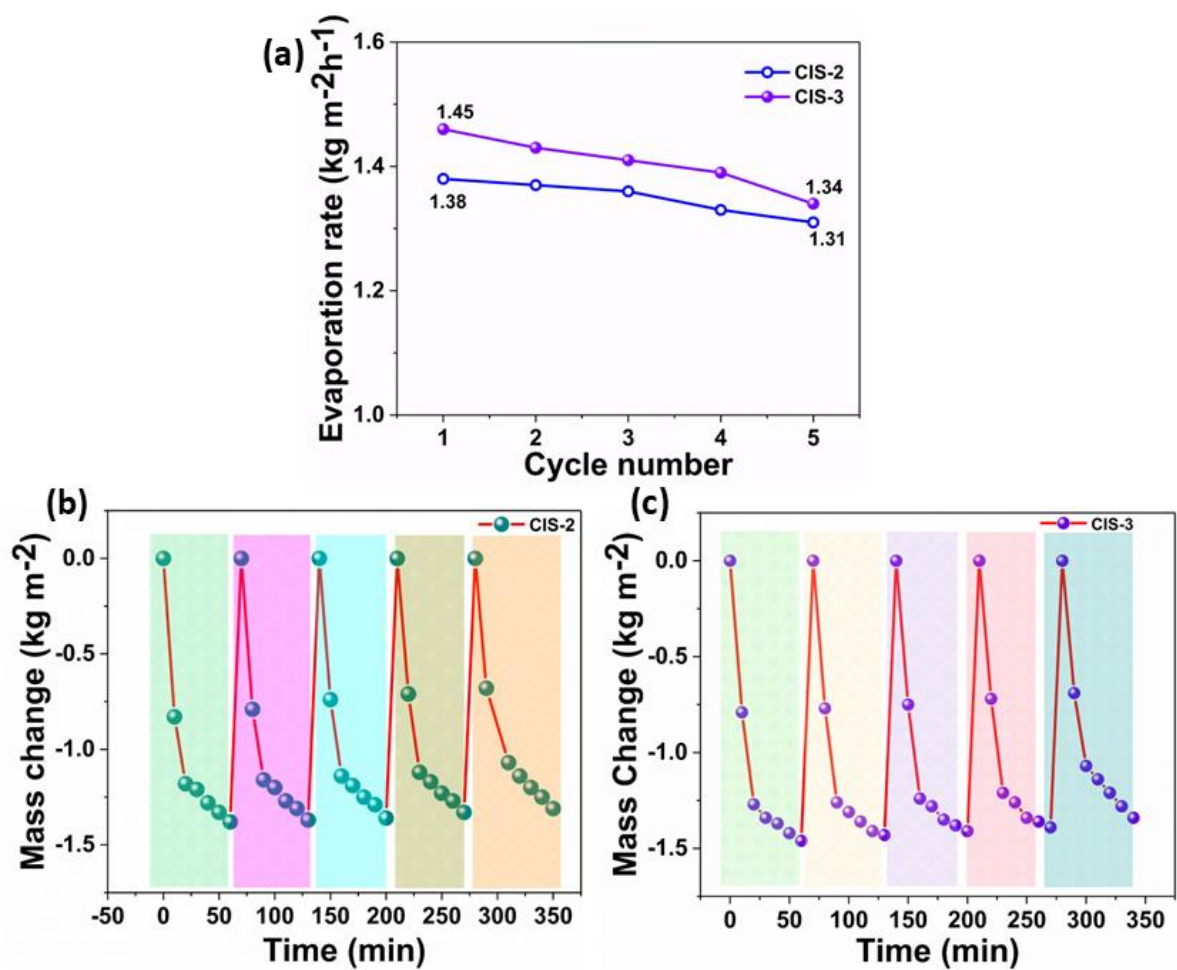


Fig. S16 (a) plot of evaporation rate vs. cycle number; cyclic stability test (b) CIS-2, and (c) CIS-3.

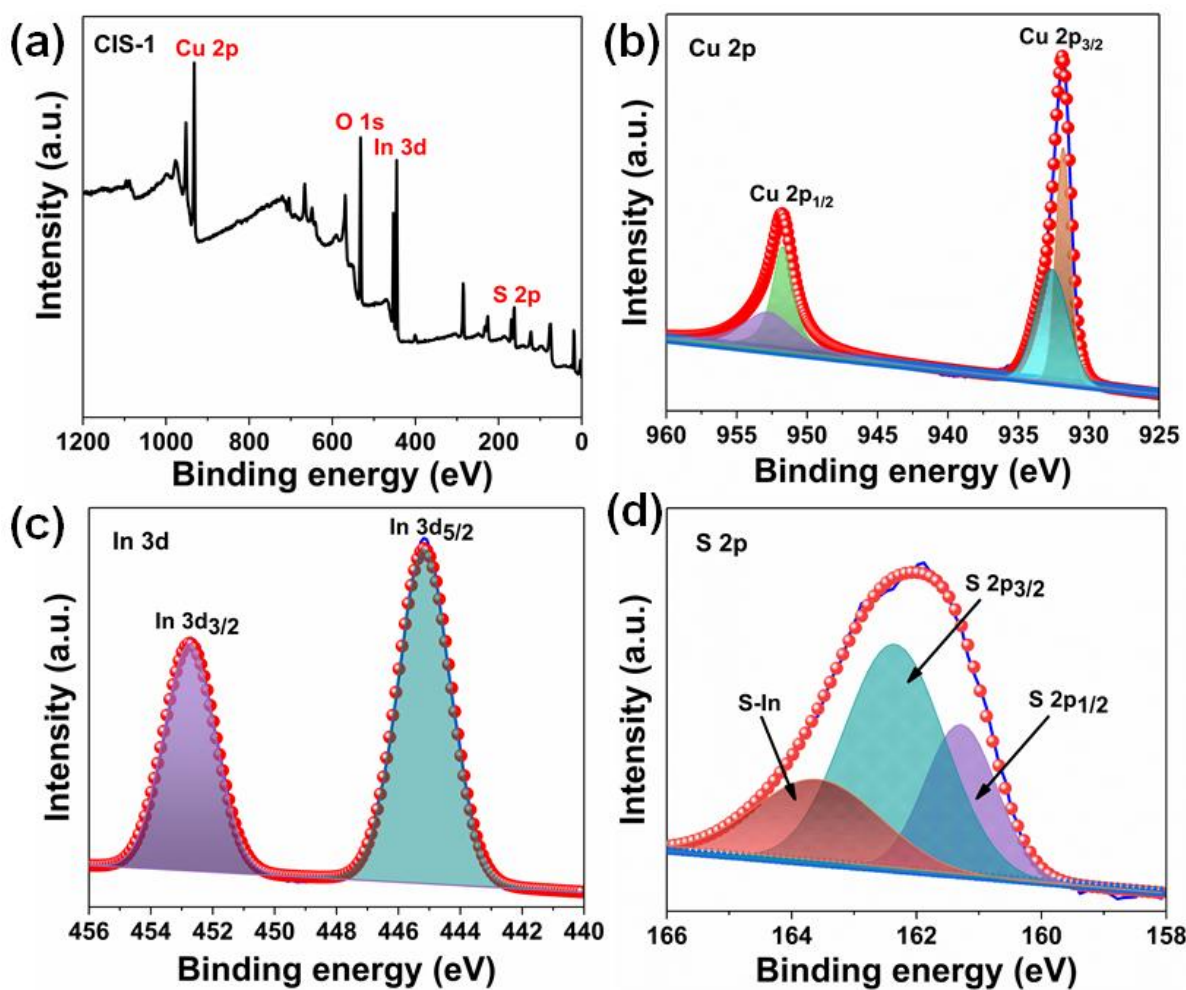


Fig. S17 (a) XPS survey spectrum of reused CIS-1, Core level deconvoluted XPS spectrum of (b) Cu 2p, (c) In 3d, and (d) S 2p, of CIS-1.

Table S1: FE-SEM and XRD results for stepwise growth pattern										
Sample	Solvent/ Soft- template	FE-SEM (morphology)			XRD					
		6 h	12 h	18 h	6 h		12 h		18 h	
					Phase	Structure	Phase	Structure	Phase	Structure
CIS-1	PEG/ Water	Irregular spherical (smaller)	Flake/ sheet	Arrays of nanoflakes	Hexagonal covellite/ tetragonal chalcopyrite	CuS/ CuInS ₂ mixture	Hexagonal covellite/ tetragonal chalcopyrite	CuS/ CuInS ₂	Tetragonal chalcopyrite	CuInS ₂
CIS-2	PEG	Irregular spherical (larger)	Sheet/ spherical	Non-spherical flower (dandelion-like)						
CIS-3	PEG/ Ethanol	Disk- shaped	Sheet/ spherical	Spherical-shaped bouquets (globe- thistle-like)						

Differential scanning calorimetry (DSC) measurements:

To support the dark evaporation process as per the reviewer's suggestion, DSC measurements were carried out at a heat flow rate of 5°C/min under a nitrogen flow of 20 mL/min. The obtained data has been tabulated in the given table.

Enthalpy(kJ/g)	Pure water	Foam	CIS-1	CIS-2	CIS-3
DSC measurement	2.41	2.12	1.28	2.15	1.85
Dark experiment	2.43	--	1.21	1.37	1.32

Sample	Turbidity (NTU)	pH
Sample water	5.88	7.3
Methylene Blue (MB)	7.62	6
Rhodamine B (RhB)	11.90	4.5
RhB/MB mixture	12	5.7
NaCl water	10.30	6.3
Fresh Water	0.94	7.2

Table S4. A comparative analysis of photothermal water evaporation of this work with previously reported studies

Sl. No	Materials	Evaporation Rate (kgm ⁻² h ⁻¹)	Solar-steam Efficiency (%)	References
1.	GO/MXene	1.27	90.7	1
2.	Co _{2.67} S ₄	2.62	82	2
3.	Al-PCP-derived porous carbon	1.72	89	3
4.	xerogel foam	3.39	95.6	4
5.	lamellar film n-PSS@CNT/rGO	1.82	97.1	5
6.	Ag/PPy	1.55	92.6	6
7.	SiC–C Composite	1.05	94.3	7
8.	iCOF	3.55	95.8	8
9.	CoCr ₂ O ₄	2.26	93.2	9
10.	MoS _{2-x} NSAs	1.32	94.2	10
11.	Cu ₂ ZnSnS ₄ nanosheets membranes	1.46	92	11
12.	Cu ₂ ZnSnS ₄ nanosheets aggregates	1.54	90	12
14.	Cu ₇ S ₄	1.41	88.1	13
15.	CuS	1.43	90.4	2
16.	Janus M-xene	1.34	90.8	14
17.	Croconium derivative	1.27	87.2	15

18.	Surface-carbonized bamboo	1.65	93.6	16
20.	(H _{1.68} MoO ₃)	1.37	84.8	17
21.	rGOMS	1.33	87.5	18
22.	SiO ₂ @CoFe/C	1.26	76.8	19
23.	ZrO ₂ -Ni@CQDs	1.95	89.5	20
24.	GO/ Cu _x S	1.56	94.6	21
25.	Polypyrrole decorated wood	1.01	72.5	22
26.	CuInS₂-1 (CIS-1)	1.55	96.8	This work
27.	CuInS₂-2 (CIS-2)	1.38	86.2	This work
28.	CuInS₂-3 (CIS-2)	1.46	91.2	This work

References

- 1 X. Ming, A. Guo, Q. Zhang, Z. Guo, F. Yu, B. Hou, Y. Wang, K. P. Homewood and X. Wang, *Carbon N. Y.*, 2020, **167**, 285–295.
- 2 F. Tao, Y. Zhang, K. Yin, S. Cao, X. Chang, Y. Lei, D. S. Wang, R. Fan, L. Dong, Y. Yin and X. Chen, *ACS Appl. Mater. Interfaces*, 2018, **10**, 35154–35163.
- 3 G. Chen, Z. Jiang, A. Li, X. Chen, Z. Ma and H. Song, *ACS Sustain. Chem. Eng.*, 2022, **10**, 4013–4021.
- 4 L. Chen, J. Ren, J. Gong, J. Qu and R. Niu, *Chem. Eng. J.*, 2023, **454**, 140383.
- 5 Y. Wu, H. Huang, W. Zhou, C. You, H. Ye, J. Chen, S. Zang, J. Yun, X. Chen, L. Wang and Z. Yuan, *ACS Appl. Mater. Interfaces*, 2022, **14**, 29099–29110.
- 6 Y. Xu, J. Ma, Y. Han, H. Xu, Y. Wang, D. Qi and W. Wang, *Chem. Eng. J.*, 2020, **384**, 123379.
- 7 L. Shi, Y. Shi, R. Li, J. Chang, N. Zaouri, E. Ahmed, Y. Jin, C. Zhang, S. Zhuo and P. Wang, *ACS Sustain. Chem. Eng.*, 2018, **6**, 8192–8200.
- 8 G. Li, Q. Yue, P. Fu, K. Wang, Y. Zhou and J. Wang, *Adv. Funct. Mater.*, 2023, **33**, 1–9.
- 9 R. Xiong, L. Zhong, Y. Song, J. Xu, Y. Xiao, B. Cheng and S. Lei, *ACS Mater. Lett.*, 2023, **5**, 1992–2001.
- 10 B. Yuan, L. Yang, H. Yang, L. Bai, W. Wang, D. Wei, Y. Liang and H. Chen, *Energy Convers. Manag.*, 2022, **252**, 115070.
- 11 C. Mu, Y. Song, K. Deng, S. Lin, Y. Bi, F. Scarpa and D. Crouse, *Adv. Sustain. Syst.*, 2017, **1**, 1–8.
- 12 J. Zhang, Y. Yang, J. Zhao, Z. Dai, W. Liu, C. Chen, S. Gao, D. A. Golosov, S. M. Zavadski and S. N. Melnikov, *Mater. Res. Bull.*, DOI:10.1016/j.materresbull.2019.110529.
- 13 X. Li, Z. Yao, J. Wang, D. Li, K. Yu and Z. Jiang, *ACS Appl. Energy Mater.*, 2019, **2**, 5154–5161.
- 14 J. Yao, Z. Zheng and G. Yang, *Nanoscale*, 2018, **10**, 2876–2886.

- 15 G. Chen, J. Sun, Q. Peng, Q. Sun, G. Wang, Y. Cai, X. Gu, Z. Shuai and B. Z. Tang, *Adv. Mater.*, 2020, **32**, 1–8.
- 16 J. Liu, J. Yao, Y. Yuan, Q. Liu, W. Zhang, X. Zhang and J. Gu, *Adv. Sustain. Syst.*, 2020, **4**, 1–8.
- 17 Q. Zhu, K. Ye, W. Zhu, W. Xu, C. Zou, L. Song, E. Sharman, L. Wang, S. Jin, G. Zhang, Y. Luo and J. Jiang, *J. Phys. Chem. Lett.*, 2020, **11**, 2502–2509.
- 18 Y. Fan, Z. Tian, F. Wang, J. He, X. Ye, Z. Zhu, H. Sun, W. Liang and A. Li, *ACS Appl. Energy Mater.*, 2021, **4**, 2932–2943.
- 19 R. Du, H. Zhu, H. Zhao, H. Lu, C. Dong, M. Liu, F. Yang, J. Yang, J. Wang and J. Pan, *Environ. Res.*, 2023, **222**, 115365.
- 20 R. T. Ginting, H. Abdullah, E. Taer, O. Purba and D. Perangin-angin, *Colloids Surfaces A Physicochem. Eng. Asp.*, 2022, **642**, 128653.
- 21 W. Sun, H. Qi, T. Li, M. Lin, C. Zhang and Y. Qiu, *RSC Adv.*, 2024, **14**, 28984–28997.
- 22 Z. Wang, Y. Yan, X. Shen, C. Jin, Q. Sun and H. Li, *J. Mater. Chem. A*, 2019, **7**, 20706–20712.